Title

Experiments on Forming, Compressing and Extracting Electron Rings for the Collective Acceleration of Ions

Authors

Keefe, D
Chupp, W W
Garren, A A
et al.

Publication Date

1970-10-01

Submitted to Nuclear
Instruments and Methods

UCRL-20144
Preprint c.2

EXPERIMENTS ON FORMING, COMPRESSING AND EXTRACTING ELECTRON RINGS FOR THE COLLECTIVE ACCELERATION OF IONS

D. Keefe, W. W. Chupp, A. A. Garren, G. R. Lambertson,
L. J. Laslett, A. U. Luccio, W. A. Perkins,
J. M. Peterson, J. B. Rechen, and A. M. Sessler

October 7, 1970

AEC Contract No. W-7405-eng-48

LAWRENCE RADIATION LABORATORY
UNIVERSITY of CALIFORNIA BERKELEY

DISCLAIMER

EXPERIMENTS ON FORMING, COMPRESSING AND EXTRACTING ELECTRON RINGS FOR THE COLLECTIVE ACCELERATION OF IONS*

D. Keefe, W. W. Chupp, A. A. Garren, G. R. Lambertson, L. J. Laslett, A. U. Luccio†, W. A. Perkins, J. M. Peterson, J. B. Rechen, and A. M. Sessler

Lawrence Radiation Laboratory
University of California
Berkeley, California 94720

October 7, 1970

ABSTRACT

In experiments related to the development of the electron-ring accelerator, electrons were injected into a pulsed magnetic field to form rings that were then compressed radially to a small size. The injected beam had a current of about 150 A at an energy of 3.3 MeV with an energy spread of ± 0.1% and a pulse length duration of 20 nsec. At low intensity, an increase in the minor radius of the ring and a large loss of electrons was observed to occur during the compression cycle. At high intensity, cooperative phenomena that caused a large increase in the energy spread accompanied by particle loss were observed. Theoretical interpretation of these observations suggests that the primary source of electron loss and enlargement of the axial dimension was the crossing of single-particle resonances during compression in the presence of large magnetic field nonlinearities and perturbations. The cooperative phenomena are interpreted as resulting from a negative mass instability. Despite the large minor radius and small number of electrons, experiments on extracting the ring were performed; under acceleration the ring failed to retain its integrity because of inadequate self-focusing.

*Supported by the U.S. Atomic Energy Commission

†At present at the Institute for Plasma Physics, Garching (Munich), Germany

1. Introduction

One form of collective-effect ion accelerator that has occupied considerable recent attention from several experimental and theoretical groups is the Electron-Ring Accelerator (ERA), in which an intense ring of relativistic electrons can serve as a vehicle to hold trapped ions while it is rapidly accelerated[1-6]. The JINR group at Dubna has reported the acceleration of nitrogen ions, by this means, to 60 MeV[7].

A critical figure of merit, for an ERA, is the peak holding field, E_p, that the trapped ion experiences in the ring, since this determines the maximum rate of ion acceleration that can be achieved. For a ring containing N_e electrons, with a major radius R, minor semi-axes, a in the radial direction and b in the axial direction, this peak holding field is given by

$$E_p = f \frac{\pi N_e e}{R(a+b)}, \qquad (1)$$

where f is a form factor of the order of unity[8]. Thus to attain rings of high quality, i.e., large E_p, requires the formation of rings with small major and minor dimensions containing a large number of electrons.

In our previous experiments, with an apparatus called Compressor 2, electron rings were formed and the quality of these rings appeared adequate for extraction of the rings and acceleration of ions. ($R = 3.5$ cm, $a \approx b \approx 2$ mm, $N_e \approx 4\times10^{12}$, $E_p \approx 12$ MV/m) (ref. [2]). Mechanically, however, Compressor 2 was not designed to accomplish these processes.

In order to extract rings and accelerate ions, an apparatus called Compressor 3 was built. Unexpected phenomena were encountered, however, in experiments with Compressor 3 that precluded the formation of rings with a quality approaching that of the rings formed in Compressor 2; viz., the rings formed in Compressor 3 were observed to have larger minor dimensions and a smaller number of total electrons. Because of the poor quality of these rings, it was not possible to extract self-focused rings and accelerate ions. This report describes the Compressor 3 equipment (sect. 2), the experimental observations (sect. 3), and how these may be interpreted theoretically (sect. 4). A brief discussion comparing the experimental results of Compressor 2 and 3 is presented in the last section (sect. 5). Clearly, a proper understanding of these phenomena and how they may be circumvented is crucial to the design of future ring-forming apparatus.

2. Experimental Apparatus

The electron source was the 4.0-MeV, 500-A Astron injector, which had been rebuilt and modified since the Compressor 2 experiments[9]). In this experiment a 3.3-MeV beam was employed. A special beam transport system containing focusing solenoid magnets and steering magnets was constructed to guide the beam from the injector to the compressor. The layout of this beam line and the compressor is shown in fig. 1. Alumina scintillators and TV cameras were used for visual-alignment observations, and air-cored toroidal transformers were used to measure electron current at various locations along the beam line.

The Astron injector produced a 300-nsec burst of electrons. A fast electromagnetic beam chopper was used to select a 20-nsec burst for delivery to the compressor, which was pulsed once every 3 sec. The emittance measuring device shown in fig. 1 not only was used to measure the emittance, but also contained instruments to collimate the beam, or to attenuate the beam by different amounts. The attenuators were carbon blocks drilled with a uniform pattern of holes and thus could reduce the intensity without changing the emittance. The phase-area acceptance of the compressor was 0.05 π cm rad. Short collimators of 2 cm and 1 cm diameter, and a long collimator of 0.6 cm diameter also could be inserted to select a central bright region with some loss of intensity.

A cross section view of Compressor 3 is shown in fig. 2. Alumina was chosen for the vacuum chamber because it is structurally strong and has good vacuum characteristics, but mostly because eddy-current effects precluded use of large areas of metal. Baking at 150°C and pumping with two 500-liter/sec ion pumps resulted in pressures between 10^{-8} and 10^{-7} torr. A liquid-helium-cooled finger (130 cm^2) was used on occasion to reduce the pressure to about one-tenth of this value.

A pulsed weak-focusing magnetic field was generated by four sets of coil pairs. Coil Sets 1A and 1B created the initial field of 700 G at injection and compressed the ring to approximately 11 cm. By adjusting the partition of current between Coils 1A and 1B, the value of the magnetic-field gradient index, $n = -\frac{r}{B_z}\frac{\partial B_z}{\partial r}$, at and soon after

injection could be varied. (The course of n values experienced at the location of the closed orbit throughout compression we will refer to as the "n trajectory".) The n value at the location of the ring could be shifted by putting a small current through a coil set which by itself would produce a large value of n at that location. In our case, a small capacitor was discharged through Coil Set 1B to shift the n trajectory at large radii. Often, two separate n-shifting circuits were used to modify n at different times during the compression cycle.

To compress the ring further, Coil Sets 2 and 3 were pulsed successively later in time. Fig. 3 shows the magnetic field, radius, and kinetic energy variation with time during a typical compression cycle. For extraction the compression cycle was modified; another capacitor bank was fired across the left coil of set number 3. This increased the field on the left and lowered the field on the right, causing the ring to roll out slowly to the right. As the voltage is raised on this extraction capacitor bank, a point is reached where the magnetic mirror on the right-hand side disappears and a rapid (nanosecond) release of the ring should have occurred with the electrons travelling rapidly to the right down the acceleration column. The image cylinder (which during extraction was located 20 cm left of the position shown in fig. 2) was used to provide additional focusing for the ring during rollout and release[10]). The image cylinder was a quartz tube 2.8 cm in radius with 36 longitudinal copper strips 0.35 cm wide and 0.0001 cm thick separated by 0.14 cm. The purpose of the copper strips was to create an electrostatic image of the ring without the magnetic image[10, 11]).

The beam was introduced into the compressor through a tapered injection pipe, or "snout," made of soft iron (to cancel the field inside) and plated with a graduated coating of copper to minimize (at the moment of injection) field perturbations of the pulsed field outside. The center of this snout was at a radius of R = 21.0 cm. The closed orbit at injection with the inflector coil off was chosen to be about 18.2 cm, corresponding to a revolution time of 3.8 nsec.

Despite precautions, the snout -- as well as other metal near the periphery of the compressor -- introduced azimuthal asymmetries in the magnetic field. Fig. 4 shows the measured asymmetry, at injection time, in the median plane for two radii. Coil Sets 1B, 2, and 3 were wound to give a threefold symmetry at the crossover point so as to minimize first and second harmonic perturbations. In fact, some third harmonic perturbation, due to the crossovers, was both observed and predicted by digital computations.

In order to inject the beam for three or four turns, a fast pulse was applied to the inflector coil (a single-turn loop at 22.5 cm radius with an associated pair of loops at 13.5 cm, as shown in fig. 2), which displaced the closed orbit at the snout from 18.2 to 21 cm and, then, during the 20-nsec pulse of beam, returned it rapidly to 18.2 cm.

The diagnostic equipment was as follows: (a) a 10-turn Rogowski belt around the snout monitored the input current to the compressor, (b) a pair of shielded Faraday cups (left-right pair) located under the snout monitored the arrival of the first few turns of beam current (inflector off), (c) a radially movable collector probe (see fig. 2) was

used to measure the total charge in the electron ring at various compression radii, (d) a calibrated magnetic pickup loop (see fig. 2) measured trapped current versus time without perturbing the ring. (e) A plastic scintillator viewed by a lead-shielded photomultiplier recorded the x rays produced when all or part of the beam struck the chamber walls or the movable obstacle probe. (f) A microwave horn and heterodyne receiver detected radiation from the ring at K-band frequency (22 GHz). Without the narrow-band receiver, high intensity microwaves in the X-band region could be detected. (g) A one-turn loop antenna (see fig. 2) with a high-pass filter detected the cyclotron frequency (≈260 MHz) and its harmonics. (h) Synchrotron light from the compressed ring traversed a sapphire window and optical system to be recorded with an image-intensifier camera having an exposure time of 500 nsec. (i) The total charge in the ring could be measured after compression by activating the rollout capacitor bank so that the ring would move to the right and strike the axially movable collector probe (see fig. 2).

3. Experimental Observations

3.1. Single-Particle Effects

Undesirable single-particle behavior in the ring-forming apparatus, or compressor, can be caused by betatron resonances which occur when the radial oscillation frequency of an electron divided by its gyrofrequency, ν_r (or the axial oscillation frequency divided by the gyrofrequency, ν_z), is a simple fraction, or when the ν_r and ν_z values are connected by simple integral relations. (See sect. 4.1. for more details.)

The importance of betatron resonances was known from the Compressor 2 experiments[2]). It was only by use of an n-shifter circuit that a large early loss was avoided in that experiment. The function of those circuits was to send a small current through a coil set which by itself would produce a large n at the position of the ring. By holding the n trajectory fairly level and postponing crossing resonances until the ring was at a small radius and hence removed from the peripheral bumps, resonances were then crossed without large amplitude growth.

The importance in Compressor 3 of an n-shifting circuit is illustrated in fig. 5. The microwave signal indicates the presence of the ring; the x-ray signal indicates electrons striking the wall or the obstacle probe, which was placed at 7 cm radius. The traces start with Coil Set 1, and large x-ray and microwave spikes occur at injection time (about 75 μsec). With the n-shifter circuit turned off, all the electrons are lost in the first 50 μsec after injection. With the n-shifter circuit switched on, electrons survive until they strike the obstacle probe at a radius of 7 cm. The loss in fig. 5(a) appears to be caused by several resonances that are traversed with a rapidly decreasing n trajectory. All data shown in the other figures were taken with one or two n-shifter circuits activated.

To study betatron resonance with a well-defined beam, which has a small n-value spread, a long collimator with a 0.6-cm-diam hole was placed in the beam line. This reduced the injected intensity to a few amperes and also, presumably, reduced cooperative effects to a negligible level. Further, the collimation reduced the axial betatron amplitude, but the radial betatron amplitude was still 2-3 cm because of the

injection-trapping mechanism. Fig. 6 shows the results of traversing the $n = 0.5$ resonance. The x-ray burst indicates loss of about 1/3 of the electrons due to that resonance. Similar behavior was observed from other resonances.

3.2. Cooperative Phenomena

After careful tuning of the Astron electron accelerator and the beam-transport system to the compressor it was found possible to transport an injected current, I_0, of typically 150 A, through the snout. The emittance of the beam that could be transported through the snout ($\approx 0.06\ \pi$ cm rad) exceeded the acceptance of the compressor ($\approx 0.05\ \pi$ cm rad). In studying intensity-dependent effects, the standard procedure was to tune the machine to obtain $I_0 \approx 150$ A, make observations, introduce attenuators that could variously give currents of $I_0/3$, $I_0/10$, or $I_0/30$, and repeat the observations.

A powerful technique for measuring radial dimensions is the observation of the burst of x rays when the beam is destroyed on the obstacle probe, namely when the electrons are successively scraped from the ring as the closed orbit moves inward during compression. In the absence of energy spread the electrons oscillate about a single closed orbit. In that case the onset of the pulse corresponds to the time of arrival of the electrons with largest betatron amplitude, and the end of the pulse corresponds to the arrival of the closed orbit when the last particle is removed. (There was no evidence of a beam that was hollow in X X' phase space.) Fig. 7 shows the onset and end times of such x-ray pulses at various radii at low beam intensity, $I_0/30$, and

it can be seen that the end points agree with the calculated curve. The shape of the pulse is a direct measure of the distribution of betatron amplitudes. If, however, the beam has a nonzero energy spread there will be a corresponding spread in the radii of closed orbits, and in this case the end of the pulse corresponds to the time of arrival of the closed orbit of the electrons with highest momentum.

We made measurements of four quantities that were observed to depend upon injected beam current: (a) ring major radius, (b) ring minor radius in the radial direction, (c) trapped ring current, and (d) radiation at the gyrofrequency and its harmonics.

3.2.1. Ring major radius

The ring major radius was measured in three ways: (a) gyrofrequency measurements, (b) synchrotron light intensity, and (c) x-ray probe measurements.

(a) Gyrofrequency measurements, with the loop antenna, gave a direct measurement of the major radius of the radiating electrons shortly after injection time. These data are presented in fig. 8.

(b) Values for the mean ring major radius can be inferred from measurement of the synchrotron light in the visible spectrum, which is rather intense at the end of compression. This intensity not only is proportional to the number of electrons in the ring but also depends critically on the energy of the electrons. These measurements showed that injection at high intensity led to a significant reduction in the energy of the compressed electrons. By use of the known history of the compression process, these measurements can be presented in

terms of a radius (and energy) shift close to injection time, as is displayed in fig. 8. The data were normalized to an 18-cm radius at 1/30 of peak intensity.

(c) Supportive evidence on this general trend was provided by observing a shift with intensity in the time of arrival of the peak of the x-ray pulse when the obstacle probe was placed at a fixed radius (see fig. 8). Since the position of the peak of the pulse depends on both the closed-orbit position and the distribution of betatron amplitudes, these data are difficult to interpret unambiguously; nevertheless the observed variation is consistent with the data just presented.

We interpret these data in terms of a rapid reduction in the mean energy of the electrons in the early history of the ring by an amount depending on the intensity of the injected beam. At full intensity this energy change is about 4%, and the corresponding mean radius change is about 1.5 cm. The question of whether this change in mean energy is accompanied by a change in energy spread is discussed later.

3.2.2. Ring Minor Radius in Radial Direction

The ring minor radius was measured by observing the time duration of an x-ray signal produced by the ring being driven, during the compression cycle, onto the movable obstacle probe. Fig. 7 shows the time of occurrence of observed signals for different probe radii, taken at a low ring intensity. At higher beam intensity (same emittance) the experimental points elongate to the left, showing an increase in minor radius in the radial direction. As shown in earlier experiments[2]), the

minor cross section of the ring was approximately elliptical with a density profile of the form

$$\frac{d^2N}{drdz} = \frac{N_e}{2\pi ab} \exp\left[-\frac{1}{2}\left(\frac{r^2}{a^2} + \frac{z^2}{b^2}\right)\right], \qquad (2)$$

where a and b are the minor radii in the radial and axial directions respectively.

Fig. 9 shows how "a" (extrapolated to maximum compression, R = 3.5 cm) varied with injected beam intensity. The results of fig. 9 indicate that a cooperative phenomenon is spreading the minor radius in the radial direction.

This is not simply an increase in betatron amplitude. As discussed above, the major radius of the ring decreased with injected beam intensity. If the electrons were to lose 4% of their energy at high injected intensity but retain their small injected energy spread, the corresponding (R, t) curve would lie about 7% below that of fig. 7. However, the locus of end points for the high-intensity case did not shift to such a curve but remained consistent with that in fig. 7 -- indicating that, despite the shift in average energy, there still remained electrons of the original energy in the beam.

Thus the decrease in major radius and increase in radial spread due to a spread in closed orbits correspond to a decrease in mean energy and an increase in the energy spread.

3.2.3. Trapped ring current

The area contained in the observed x-ray pulses, after suitable calibration, can be used as a measure of the total amount of beam surviving until destruction by the obstacle probe. This was measured at several radii as a function of beam intensity, and the results are shown in fig. 10. The data points have considerable scatter, but an average of least-squares fits to the data for each radius indicates that in going from low to high intensity the proportion of electrons circulating in the ring drops by about 30%. Despite the large fluctuations in this sequence of measurements, one can infer that the loss due to high intensity effects is not a dramatic one.

3.2.4. Radiation at gyrofrequency and its harmonics

Radiation from the ring at the electron cyclotron frequency (ω_{ce}) and its harmonics was observed to be greatest near injection time. Fig. 11 shows the signal detected by the loop antenna (ω_{ce} region) and with an X-band microwave detector (25 to 50 ω_{ce} region). The signals reach maximum amplitude in a few nsec and decrease to a small value in about 75 nsec. The loop-antenna signal actually lasts for several microseconds, but at a much lower level.

A search was made, using the signal from the loop antenna and a set of pass-band filters for radiofrequency radiation at frequencies that might correspond to $|(\nu \pm m)\omega_{ce}|$, where ν is either the axial or radial betatron tune and m is a small integer or zero. No such frequencies were detected, and the antenna signal was dominated by the cyclotron frequency for some time after injection.

Mindful that cooperative phenomena are strongly dependent upon the energy spread in the ring, we measured the energy spread of the injected beam and attempted, furthermore, to increase the Landau damping of any cooperative instabilities by increasing this energy spread. The incident energy spread was measured by using the compressor as a 340-deg spectrometer. The snout was stopped down to a narrow slit; the field index, n, was adjusted to give an image of this slit on the Faraday cups (340 deg away in azimuth); and the charge collected was observed as a function of the magnetic field. Pulse-to-pulse jitter set a limit of $\frac{\Delta p}{p} \approx \pm 0.1\%$, and we concluded that the instrinsic energy spread was, at most, of this order. (This was a surprising result, since measurements with Compressor 2 had given $\frac{\Delta p}{p} = \pm 0.25\%$; the difference could be attributed to the fact that the Astron accelerator had been completely rebuilt in the time period between the Compressor 2 and Compressor 3 experiments.)

In an attempt to introduce instantaneous energy spread into the injected beam, a thin energy-loss foil of irregular thickness was introduced at the exit end of the accelerator. Coulomb scattering resulted in a large increase in emittance and the beam entering the compressor was reduced below usable limits. As an alternative, certain of the accelerating cores were phased back to create an energy variation in time corresponding to a change of 1% per turn. Whether such a sweeping in energy without significant instantaneous spread generates significant Landau damping is highly dubious. In any event, no change in the ring behavior was detected with this mode of operation.

A further attempt to change the Landau damping was made with the n-shifter circuits. Although they were primarily intended to modify the n trajectory, their activation also produced a change in the derivative $\frac{\partial n}{\partial r}$ close to injection time, leading to different n values experienced by electrons of different momenta. The value of $\frac{\partial n}{\partial r}$ at injection was varied from + 0.025 cm^{-1} to - 0.025 cm^{-1} without any obvious effect on the ring behavior.

Collective behavior is expected to be strongly dependent upon the electrical environment of the ring. The interior ceramic surfaces were plated with a conducting layer of about 150 Ω/square, but a check at the end of the experiment showed that the layers seemed to have lost, almost completely, their conductivity. Thus, unfortunately, the experiment may have been performed under poor conditions; and, at the least, the actual conditions are unknown, which introduces a further uncertainty into the interpretation of the results.

3.3. High-Intensity Results

Experiments at high intensity were typically done with an uncollimated injected beam of 150 A or a collimated (2 cm diam) beam of lower emittance and 80 A. If three turns were trapped at 100% efficiency then the 150-A beam would produce a ring containing 1.1×10^{13} electrons. However, from the experience with Compressor 2, we would expect about a 40% trapping efficiency.

Measurements of N_e versus time are shown in fig. 12. All these data were taken with a 2-cm collimator in the beam line, except for the magnetic-pickup-loop data marked "full beam" on the figure (150 A).

The magnetic-pickup-loop data represent an average of many pulses. We believe the magnetic-pickup-loop gives the correct absolute value, whereas the radial collector and axial collector give a low value because of secondary-electron emission.

Both the magnetic-pickup-loop and radial-collector data show a large electron loss during the first 60 μsec. In contrast, the Compressor 2 magnetic-pickup-loop data showed a nearly constant N_e versus time. Apparently, this loss is not due to a cooperative effect, because at a current level of $I_0/3$ the magnetic-pickup-loop signal had the same relative decrease with time, but with 1/3 lower initial amplitude. Also, the signal from the axial collector, measured after ring compression, decreased in proportion to the injected beam intensity. For a cooperative loss, the result should be very different. All these variations in injection current were done at constant emittance. However, the "full beam" had a larger emittance than the "2-cm beam," and the results in fig. 12 show that the particles with larger betatron amplitudes are more readily lost.

The movable collector probe consisted of a stainless steel flag that was mounted on a radial shaft that entered from the outermost radius of the compressor and was well to the side of the expected ring position (see fig. 2). Nevertheless, with the flag at very small radii out of the beam, the presence of the shaft produced large beam loss, as evidenced by the x-ray monitor. This observation is an indication of strong axial spreading of the high-intensity beam.

Table 1 shows a comparison of the electron rings formed in Compressor 2 and in Compressor 3. The radial minor radius was measured

by the x-ray-probe method (see sect. 3.2.2) and synchrotron light method.[2] The visible synchrotron light for these energies is a rapidly varying function of the electron energy. Because of the energy spread in Compressor 3, the radial minor radius measured by this method may be too small, thus explaining the discrepancy with the x-ray-probe data. The axial width of the ring was measured by use of an obstacle probe and x-ray detector as well as using the synchrotron-light method. The main differences between Compressors 2 and 3 are N_e at 90 μsec and the axial width b. We attribute the decrease of N_e between 10 and 90 μsec and the large b after compression to betatron resonance growth in Compressor 3.

3.4. Extraction of Ring

Despite the poor ring quality achieved in Compressor 3, attempts were made to extract the ring axially. At the time of peak compression a capacitor bank was discharged so as to increase the current in the left-hand solenoid of Coil Set 3 and decrease the current in the right-hand solenoid. This unbalancing circuit was critically damped so that the magnetic field would return to its usual symmetry in a few hundred μsec. By this method it was possible to roll the electron ring to various distances to the right of the midplane and have it return.

As the ring moved to the right of the midplane it moved from a region with n = 0.1 toward a region of n = 0 (the point of release). By increasing the unbalance current it was possible to expose the ring to successively lower values of n and then bring it back to the midplane to note the change. (As n is brought closer to zero, the $\nu_r = 1$ and $\nu_z = 0$

resonances are approached with possible passage through the $\nu_r = 1$ resonance. Both ν_r and ν_z are of course modified by ion loading and the presence of an image cylinder.)

The ring survived this motion until the unbalance current was great enough to push it to the release point. The ring was then observed to strike a probe about 10 cm to the right of the release point. From the long signal (several μsec) it was observed that the ring did not move as an integral unit, but that betatron amplitudes peeled off axially as they reached the release point.

There was no evidence of a resonance loss during this stage unless it occurred exactly at the release time. Neither ion loading nor the presence of an image cylinder inside the ring affected the time of the release signals, giving evidence that the signals were not caused by a resonance loss.

4. Interpretation of Observations

4.1. Betatron Resonances

The radial and axial betatron tunes ν_r and ν_z are related (for single particles and without image forces) to the field gradient n by

$$\nu_r^2 = 1 - n ,$$

$$\nu_z^2 = n . \qquad (3)$$

In the course of the compression cycle (see fig. 3), there are a number of potentially dangerous resonances which can be encountered:

$$
\begin{aligned}
2\nu_r &= 2\nu_z, && \text{at } n = 0.5;\\
2\nu_z + \nu_r &= 2,, && \text{at } n = 0.36;\\
2\nu_z &= 1 && \text{at } n = 0.25;\\
2\nu_z &= \nu_r, && \text{at } n = 0.20. \qquad (4)
\end{aligned}
$$

Presumably less important, and hence not included in Eq. (4), are higher-order resonances, and those occurring in fields with non-median-plane symmetry, as the compressor was designed to have median-plane symmetry (and the magnetic measurements indicated that the deviations from this symmetry were small).

Because the ring is formed by injection of three turns in the radial direction, the radial betatron amplitude is greater than the axial betatron amplitude. The effect of all these resonances is to increase the axial betatron amplitudes. This can lead to an undesirably large minor radius axially and to particle loss on the compressor walls.

The resonances at n = 0.5 and n = 0.2 are similar. They will occur in magnetic fields with no azimuthal asymmetries, as they are driven by nonlinearities of the magnetic field, namely, $(\partial^2 B_z/\partial r^2)$ and $(\partial^3 B_z/\partial r^3)$, etc. In contrast, the n = 0.36 and n = 0.25 resonances are driven by azimuthal asymmetry of the magnetic field.

Analytic and computer calculations have been made of the effect of crossing the above-listed resonances[12]). The computer calculations employed magnetic fields which simulated those actually present in the experimental apparatus; that is, the input to the computer consisted of magnetic fields at various times during the compression cycle. In

fig. 4 is an example of the perturbation fields employed.

One result of these computational studies was that for the n = 0.5 resonance the radial amplitude squared plus the axial amplitude squared is approximately constant for each particle (unless the radial amplitudes are extreme). Four times the square of the radial amplitude plus the square of the axial amplitude is the conserved quantity for the n = 0.20 resonance. Although the damage that these two resonances can cause is thus somewhat limited, the mixing of radial and axial betatron amplitudes is not, in general, desirable.

Computational studies were made of the effect of crossing the resonances listed by eqs. (4). An example of the results is presented in fig. 13, where a particle of initial radial amplitude 1.5 cm is taken through the n = 0.5 resonance.

In the experiment, trajectories typically traversed the n = 0.5 resonance under conditions which, according to the computations, should have caused a large increase in the axial dimension of the ring and particle loss if the radial amplitude were greater than 2.0 cm. Such loss was in fact observed, as may be seen in fig. 6.

During the experiment, trajectories staying below n = 0.5 and below n = 0.36 were also tried but failed to reduce the particle loss. Computer calculations with some of these trajectories showed that it would be disastrous to cross n = 0.36, or n = 0.25, or n = 0.20 at large radii ($R > 15$ cm). The computer calculations indicated, however, that at smaller radii ($R < 12$ cm), only small amplitude growth would occur. In principle, by using n shifters, it should have been possible

to steer clear of these resonances until smaller radii were reached.

However, under high-current conditions cooperative phenomena led to a spread in closed-orbit radii and consequently to a spread in n trajectories when a dynamic n shifter is used. This spread in n trajectories ($\Delta n \approx 0.1$) presumably made it impossible to find a path that avoided crossing a resonance at a large radius, where the perturbations and nonlinearities were relatively large. Furthermore, a spread in closed orbits leads to a spread in the time at which a resonance is crossed and hence to a dilated loss pattern in the x-ray signal, which is in accord with the observations on high-current rings.

4.2 Negative-Mass Instability

Azimuthal bunching of the electrons in a ring will be unstable if the spread in gyrofrequency of electrons is too small. Such an instability has been observed in a variety of devices[13-16]. The threshold [i.e., the critical number of electrons, $(N_e)_{th}$, below which the negative mass instability does not occur] is given by[17,18]

$$(N_e)_{th} = \frac{\pi}{2}\left(\frac{R}{r_0}\right)\left(\frac{\gamma}{g}\right)\left[-\frac{E}{\omega_{ce}}\frac{d\omega_{ce}}{dE}\right]\left(\frac{\Delta p}{p}\right)^2 , \qquad (5)$$

where R is the ring major radius, r_0 is the classical electron radius, γ is the ratio of total electron mass to rest mass, $(\Delta p/p)$ is the fractional momentum spread (full width at half maximum), ω_{ce} is the gyrofrequency, E is the total energy, and g is a factor that relates the azimuthal electric field to the bunching. In an azimuthally uniform field and for $\gamma >> 1$, we have

$$-\frac{E}{\omega_{ce}}\frac{d\omega_{ce}}{dE} \approx \frac{1}{1-n} , \tag{6}$$

where n is the field index.

The geometrical factor, g, is a function of the nature and location of the material near the ring. For a ring of minor radius a, located on the midplane between two perfectly conducting planes separated by the distance H, the factor g is given by[19]

$$g = \frac{1}{\gamma^2}\left[1 + 2\ln\left(\frac{2H}{\pi a}\right) + \left(\frac{H}{\pi R}\right)^2\right] , \tag{7}$$

provided the mode number ℓ satisfies

$$\ell << n_1 , \tag{8}$$

where the mode number ℓ is related to the perturbation wavelength λ by

$$\ell = 2\pi R/\lambda , \tag{9}$$

and

$$n_1 \equiv \frac{\pi R}{H} . \tag{10}$$

The last term in eq. (7) is a curvature -- or coherent radiative -- term. In the limit of $n_1 >> \gamma$, eq. (7) reduces to the more usual approximation for g--namely the first term of eq. (7)[17]. When ℓ is comparable to or larger than n_1, then g must be evaluated numerically[19].

For the case in which an electron ring is surrounded by a closed conducting cavity, the factor g exhibits resonances[20,21]), and the same type of behavior also occurs if the surrounding material is dielectric[22]).

We may employ eqs. (5) and (6) to gain insight into the experimental situation in Compressor 3. Solving for the momentum spread necessary to stabilize $N_e = 4\times10^{12}$ electrons yields (after inserting R = 18 cm, $\gamma = 7.6$, and $n = 0.5$),

$$\frac{\Delta p}{p} \geq 5\times10^{-2}\, g^{\frac{1}{2}} \quad . \tag{11}$$

If we employ eq. (7), taking H = 5 cm and a = 2 cm, then $g = 0.041$ and the threshold condition becomes $(\Delta p/p) \geq 1.0\%$. For mode numbers ℓ comparable to n_1 we employ the numerical results of ref. [19]) to obtain the maximum g value (at mode $\ell \approx 35$) of $g = 0.094$, and hence a required $(\Delta p/p) \geq 1.5\%$.

However, the walls of Compressor 3 were ceramic with a low- or zero-conductivity coating, as was discussed in sect. 3.2. Therefore, computations for ceramic surroundings (ref. [22]) are most pertinent, even though in this work the analysis is restricted to cylindrical geometry. Neglecting curvature effects but including ceramic effects should not be a serious compromise.

Numerical studies of the effect of conducting layers of various surface conductivity superimposed on ceramic indicate that the threshold $(\Delta p/p)$ increases rapidly as the surface resistivity is increased. The variation of the threshold $(\Delta p/p)$ for several wall conductivities is

given (for a representative cylindrical geometry) in table 2.

Thus, since the injected energy spread in the experiment was $\approx$ 0.2% and the wall resistivity was -- at best -- 150 Ω/sq, one could expect, theoretically, a strong negative mass instability under full-current operation.

The behavior of negative mass-unstable beams has been studied experimentally[13,15]), and it was found that the beams self-stabilize after increasing their energy spread. Quasi-linear theory[23]) as well as computational studies[24,25]) predict self-stabilization, in agreement with the experiments. One computational study shows that if the initial energy spread is very small, then the energy spread after self-stabilization is considerably larger than the threshold value for a uniform beam.[24]) Since the experimentally measured initial momentum spread was below even the lowest theoretical threshold estimate, this instability could have caused the significant increase in momentum spread that was observed.

4.3. Criteria for Ring Integrity During Extraction

In order to have a ring extracted as a unit, the self-focusing forces must be large enough to satisfy certain inequalities involving the energy spread in the ring and the spatial derivatives of the radial magnetic field.[26]) For the parameters of our apparatus, the inequalities are essentially equivalent to requiring positive axial focusing; namely

$$\nu_z^2 > 0 . \qquad (12)$$

During extraction the field index n becomes very small and the formulas of eq. (3), for ν_r^2 and ν_z^2, are inadequate. Including the effects of electron repulsion, ion focusing, and image focusing, the betatron tunes are given (for $\beta \approx 1$) by[27]

$$\nu_r^2 = 1-n-\left\{\frac{4R^2}{a(a+b)}\left(\frac{1}{\gamma^2}-f\right)-(1-f)\frac{P}{2}+8(\epsilon_e/U)(1-f)\left[(1-K^2U)^{-\frac{1}{2}}-1\right]\right.$$

$$\left.-8(\epsilon_m/U)\left[(1-L^2U)^{-\frac{1}{2}}-1\right]+n\left[\left(1-\frac{f}{2}\right)P+(1-f)K-L\right]\right\}\mu \quad (13)$$

and

$$\nu_z^2 = n+\left\{-\frac{4R^2}{b(a+b)}\left(\frac{1}{\gamma^2}-f\right)-(1-f)\frac{P}{2}+8(\epsilon_e/U)(1-f)\left[(1-K^2U)^{-\frac{1}{2}}-1\right]\right.$$

$$\left.-8(\epsilon_m/U)\left[(1-L^2U)^{-\frac{1}{2}}-1\right]+n\left[\left(1-\frac{f}{2}\right)P+(1-f)K-L\right]\right\}\mu\,, \quad (14)$$

where

$$K \approx \frac{1}{S_e-1}\,;\quad L \approx \frac{1}{S_m-1}\,;\quad U=\frac{a^2-b^2}{4R^2}\,, \quad (15)$$

and S_e = (radius of cylinder for electrical images)/R ,

S_m = (radius of cylinder for magnetic images)/R,

$\mu = N_e r_0/(2\pi R\gamma)$,

$f = Z_i N_i/N_e$, and

$P = 2\ln[16R/(a+b)]$

In the above equations, N_i is the total number of ions and Z_i is the charge state of the ions. The electrostatic and magnetostatic image-

field coefficients, ϵ_e and ϵ_m, for a conductor equal 0.125. These equations are for a ring with a uniformly populated elliptical minor cross section. The value of a and b for a Gaussian ring (see eq. 2) should be roughly doubled when used in these formulas.

The different focusing forces contributing to eqs. (13) and (14) have the sign shown in Table 3. Thus the linear and toroidal space-charge terms, caused by other electrons, are defocusing axially while the ion and image-focusing terms are focusing axially. The purpose of image focusing is to form a positive electrostatic image (in a cylinder either outside or inside the ring) with no magnetic image. This can be achieved by using a cylinder formed of slotted-metal conductor[11]) or (for low $\beta_\perp$) a dielectric cylinder[28]). Slotted-metal cylinders can give values of ϵ_e close to 0.125; dielectric cylinders typically give values of ϵ_e from 0.08 to 0.11. A slotted-metal cylinder (see fig. 2) was used for most of the Compressor 3 experiments.

When the ring is moved into the $n \approx 0$ field region, a tune shift will occur and cause both a and b to change. The change is evaluated by use of the betatron phase-space invariants

$$\beta\gamma a^2 \nu_r/R = C_r = \text{constant}, \tag{16}$$

$$\beta\gamma b^2 \nu_z/R = C_z = \text{constant}. \tag{17}$$

As n approaches zero, the axial width will increase, causing weaker axial focusing, which in turn causes a further increase in axial width. Therefore, using values of a and b in the field region where

$n = 0.1$, we have solved eqs. (13), (14), (16), and (17) simultaneously for (a, b, ν_r^2, ν_z^2) by an iterative process. For Compressor 3 we have taken $\gamma = 32.3$ (kinetic energy = 16 MeV) and $R = 3.5$ cm (in the $n = 0.1$ region) and $R = 3.3$ cm (in the $n = 0$ field region).

Fig. 14 shows curves of the minimum number of electrons versus b for three values of a and $f = 0.25$ (but without image focusing). For a given value of a, the ring can hold together during extraction only if the point (N_e, b) is above the curve. As one can see from the graph, the minimum N_e depends strongly on b. The quality of the rings formed in Compressor 3 was such that they should not hold together during extraction, as the (N_e, b) value is far below the curves.

Fig. 15 shows curves of the minimum number of electrons versus b for two values of a, $f = 0$, and a slotted-metal image cylinder 0.5 cm from the center of the ring. (Note that a must be less than the separation of the image cylinder and ring, since particles with large amplitude will be wiped off on the image cylinder.) An image cylinder 0.5 cm from the center of the ring gives an axial focusing equivalent to about 50% ion loading. Thus, with the rings that were obtained in Compressor 3, the axial spreading after release can be well understood.

5. Discussion of Compressors 2 and 3

The experiment described herein followed previous work on Compressor 2, in which we had been successful in making rings having high current and small minor dimensions. Such rings should be suitable for extraction (see figs. 14 and 15). It was, in fact, the previous success which motivated constructing Compressor 3 with its potential

capability for extracting rings and accelerating ions. But, as we have described in this report, we were not successful in the Compressor 3 experiments in making rings of adequate quality for extraction and acceleration.

We believe that the difficulties encountered in Compressor 3 were caused by two effects: (a) single-particle resonances and (b) an azimuthal instability. The single-particle resonances were presumably driven by large azimuthal field perturbations and large nonlinearities in the variation of the magnetic field with radius. The azimuthal instability could have been caused by inadequate conductivity of the ceramic surfaces near the beam, or by the exceedingly small momentum spread in the initial beam (either leading to an excessive momentum spread in the ring before self-stabilization), or by both effects.

In comparing this experiment with Compressor 2 we find that single-particle resonances were not nearly so important in Compressor 2; theoretical computations, using the Compressor 2 fields, predict very little beam loss or growth in ring minor dimensions for that experiment. Furthermore, in the Compressor 2 experiment the initial momentum spread was larger than in Compressor 3; and, finally, the walls of Compressor 2 may well have had significantly higher conductivity than those of Compressor 3. (In both cases the interior ceramic surfaces were plated with a conducting layer of about 150 Ω/square. A check at the end of the Compressor 2 experiment showed that on one of the ceramic side plates the thin nickel coating was still continuous, whereas on the other side plate it was not. At the end of the

Compressor 3 experiment the thin gold coating on both side plates was found to be broken up into small, unconnected islands. The times at which the conducting coatings lost their integrity are uncertain in each case.)

Finally, we remark that it is important for the successful formation of electron rings of high quality to understand the difficulties that were encountered in the present experiment. Our group is now engaged in experiments with Compressor 4 that are addressed specifically to this end. When a better understanding of the creation of high-quality rings is obtained, efforts to extract and accelerate ion-loaded rings will be renewed.

ACKNOWLEDGMENTS

The constant interest and encouragement by E. M. McMillan and E. J. Lofgren are greatly appreciated. We are deeply indebted for the unique contributions by R. W. Allison, R. T. Avery, J. S. Colonias, A. C. Entis, A. Faltens, D. R. George, H. A. Grunder, E. C. Hartwig, J. M. Hauptman, R. N. Healey, H. P. Hernandez, H. D. Lancaster, B. S. Levine, A. J. Nakach, C. Pellegrini, W. W. Salsig, Jr., and P. B. Weiss.

Without the devotion and unusual skills, in the area of mechanical construction, of J. R. Meneghetti and his team, and the outstanding and enthusiastic efforts in the electrical installations by C. D. Pike and his group, these experiments would not have been possible. We are also thankful for the valuable cooperation of C. M. Van Atta, T. K. Fowler and N. C. Christofilos, and the members of the Astron accelerator group.

REFERENCES

1. V. I. Veksler et al., Cambridge Electron Accelerator Report No. CEAL-2000, p. 289; 1967.

2. D. Keefe et al., Phys. Rev. Letters 22 (1969) 558.

3. D. Keefe, in Proceedings of the 1969 Particle Accelerator Conference, IEEE Trans. Nucl. Sci. NS-16, No. 3, June 1969, p. 25.

4. V. P. Sarantsev, in Proceedings of 1969 Particle Accelerator Conference, IEEE Trans. in Nucl. Sci. NS-16, No. 3, June 1969, p. 15.

5. C. Andelfinger et al., Status Report on Electron Ring Experiments in Garching, in Contributions to the 3rd Work Meeting on Electron Ring Accelerators, Kernforschungszentrum Karlsruhe Report 3/69-30, October 1969.

6. P. Kappe, The Karlsruhe Compressor, ibid.

7. V. P. Sarantsev, in Proceedings of the VII International Conference on High Energy Accelerators, Erevan, USSR, 1969, (to be published).

8. See, for example, Symposium on Electron Ring Accelerators, Lawrence Radiation Laboratory Report UCRL-18103, 1968 (unpublished). Also see C. Bovet, Holding Field of a Non-Uniformly Charged Electron Ring, Lawrence Radiation Laboratory Report ERAN-88. June 1970 (unpublished).

9. J. W. Beal, N. C. Christofilos, and R. E. Hester, in Proceedings of the 1969 Particle Accelerator Conference, IEEE Trans. in Nucl. Sci. NS-16, No. 3, June 1969, p. 294.

10. See Ref. 8, p. 140 and p. 383.

11. G. V. Dolbilov et al., in Proceedings of the VII International Conference on High Energy Accelerators, Erevan, USSR, 1969, (to be published).

12. L. J. Laslett and W. A. Perkins, Betatron Amplitude Growth Upon Traversing Resonances During the Compression Cycle of an Electron Ring Accelerator, Lawrence Radiation Laboratory Report UCRL-20143, 1970 (to be published).

13. M. Q. Barton and C. E. Nielsen, in Proceedings of the International Conference on High Energy Accelerators, Brookhaven, 1961 (U.S.A.E.C., Washington, 1961), p. 163.

14. G. R. Lambertson, in Proceedings of an International Conference on High Energy Accelerators, Dubna, 1963 (Atomizdat, Moscow, 1964) p. 153.

15. H. Postma, J. L. Dunlap, R. A. Dory, G. R. Haste and R. A. Young, Phys. Rev. Letters 16 (1966) 265.

16. J. W. Beal, R. J. Briggs, R. E. Hester, E. J. Lauer and P. B. Weiss, Bull. Am. Phys. Soc. 11 (1966) 565.

17. C. E. Nielsen, A. M. Sessler and K. R. Symon, in Proceedings of the International Conference on High Energy Accelerators Instrumentation, 1959, L. Kowarski, ed. (CERN Scientific Information Service, Geneva, 1959), p. 239.

18. A. A. Kolomenskii and A. N. Lebedev, Soviet J. At. Energy (English Transl.) 7 (1961) 1013.

19. C. Pellegrini and A. M. Sessler, in Symposium on Electron Ring Accelerators, Lawrence Radiation Laboratory Report UCRL-18103, 1968, p. 442 (unpublished).

20. A. G. Bonch-Osmolovskii and E. A. Perel'shtein, Longitudinal Instabilities in Circular Charged Beams, Part I. Effect of Negative Mass, Joint Institute for Nuclear Research Preprint P9-4424, 1969, Lawrence Radiation Laboratory Translation 1402, Nov. 1969; A. G. Bonch-Osmolovskii and E. A. Perel'shtein, Longitudinal Instabilities in Circular Charged Beams, Part II. Radiative Instability, Joint Institute for Nuclear Research Preprint P9-4425, 1969, Lawrence Radiation Laboratory Translation 1403, Nov. 1969.

21. A. Entis and L. Smith, Negative Mass Instability in a Pillbox Cavity, Lawrence Radiation Laboratory Report ERAN-100, August 1970 (unpublished).

22. B. Zotter, Stability of Electron Rings in Ceramic Compressor Chambers, in Contributions to the 3rd Work Meeting on Electron Ring Accelerators, Kernforschungszentrum Karlsruhe Report 3/69-30, October 1969; B. Zotter, Longitudinal Instability of Relativisitc Particle Beams in Laminated Vacuum Chambers, CERN Report IRR-TH/69-35, June 1969.

23. E. A. Perel'shtein, Quasilinear Theory of Longitudinal Space-Charge Effect in Particle Accelerators, in Proceedings of V International Conference on High Energy Accelerators, Frascati, 1965 (CNEN, Roma, 1966), p. 362.

24. R. A. Dory, Nonlinear Azimuthal Space Charge Effects in Particle Accelerators, Midwestern University Research Report MURA-654, Aug. 1962 (unpublished).

25. M. S. Grewal and J. A. Byers, Plasma Physics 11 (1969) 727.

26. C. Pellegrini and A. M. Sessler, Lower Bounds on Self-Focusing So As to Maintain Ring Integrity Near the Initiation of Acceleration in an Electron Ring Accelerator (Lawrence Radiation Laboratory Report UCRL-19398 Rev., April 1970) Nucl. Instr. and Methods (to be published).

27. L. J. Laslett, On the Focusing Effects Arising From the Self-Fields of a Toroidal Beam, Lawrence Radiation Laboratory Report ERAN-30, April 1969 (unpublished); L. J. Laslett, Image Field of a Straight Beam of Elliptical Cross Section, Lawrence Radiation Laboratory Report ERAN-49, January 1970 (unpublished).

28. L. J. Laslett, Enhancement of Incoherent Ring-Image Focusing Through Use of Dielectric, in Symposium on Electron Ring Accelerators, Lawrence Radiation Laboratory Report UCRL-18103, 1968, p. 426 (unpublished).

Table 1. Comparison of ring parameters

	Compressor 2	Compressor 3
N_e at 10 μsec	2 to 4×10^{12}	2 to 4×10^{12}
N_e at 90 μsec	2 to 4×10^{12}	1×10^{12}
a (synchr. light)	0.24 cm	0.24 cm
a (1/4 beam)	0.25 cm	0.3 cm
a (full beam)	-----	0.6 cm
b (synchr. light)	0.16 cm	0.5 cm
b (full beam)	0.15 to 0.3 cm	0.5 cm

Table 2. Threshold momentum spread for various wall resistivities for typical Compressor 3 parameters

Wall resistivity (ohm/square)	$(\Delta p/p)_{th}$ (%)
0	1.0
10	2.3
100	3.6
1000	9.6

Table 3. Sign of focusing forces (near $\nu_z = 0$).

	ν_r^2	ν_z^2
linear space charge	-	-
"toroidal" space charge	+	-
ion focusing	+	+
image focusing	-	+

FIGURE CAPTIONS

Fig. 1. Experimental layout of the injector, beam line and compressor.

Fig. 2. Cross section view of the compressor.

Fig. 3. The major radius (R) of the ring, the kinetic energy (T) of the electrons, the magnetic field (B) and the magnetic field index (n), at the ring, as functions of time during the compression of the ring for a typical compression cycle.

Fig. 4. The variation of the z component of magnetic field as a function of azimuthal angle for radii of 18.5 cm and 13 cm at the time of injection.

Fig. 5. Microwave signal (nondestructive indication of presence of beam) and x-ray signal (indication of beam loss) showing the effect of an n shifter on betatron resonance loss.

Fig. 6. X-ray signal showing electron loss on traversal of $n = 0.5$ resonance.

Fig. 7. Radius of the electron ring versus time showing experimental points with the injected beam intensity attenuated to 1/30 of its normal value.

Fig. 8. Variation of ring radius (extrapolated back to the time of injection) as a function of the injected beam intensity.

Fig. 9. Minor radius of ring in radial direction (rms value) for a Gaussian distribution [see Eq. (2)] extrapolated to the final compression radius, as a function of the injected beam intensity.

Fig. 10. The trapped beam intensity as a function of the injected beam intensity. The dashed line is a linear variation; the solid curve is the average of least-squares fits of the experimental points to the function $Y = AX + BX^2$.

Fig. 11. Signals from the X-band detector and loop antenna near injection time.

Fig. 12. Experimental measurements of the number of electrons in the ring versus time. All these data, except the curve marked marked "Full beam," were taken with the injected beam collimated by a 2-cm-diam hole.

Fig. 13. Radial and axial betatron amplitudes versus time as the $n = 0.5$ resonance is traversed by a particle in a computer calculation. The initial radial and axial betatron amplitudes are 1.5 cm and 0.1 cm respectively. The top graph shows how n is varying during this time.

Fig. 14. Curves of the minimum number of electrons to hold a ring together as a function of b for a = 0.2, 0.75, and 1.5 cm; f = 0.25.

Fig. 15. Curves of the minimum number of electrons to hold a ring together as a function of b for a = 0.2 and 0.5 cm; f = 0. An image cylinder with $\epsilon_e = 0.125$ and $\epsilon_m = 0$ is inside the ring (R = 3.3 cm) at a radius of 2.8 cm.

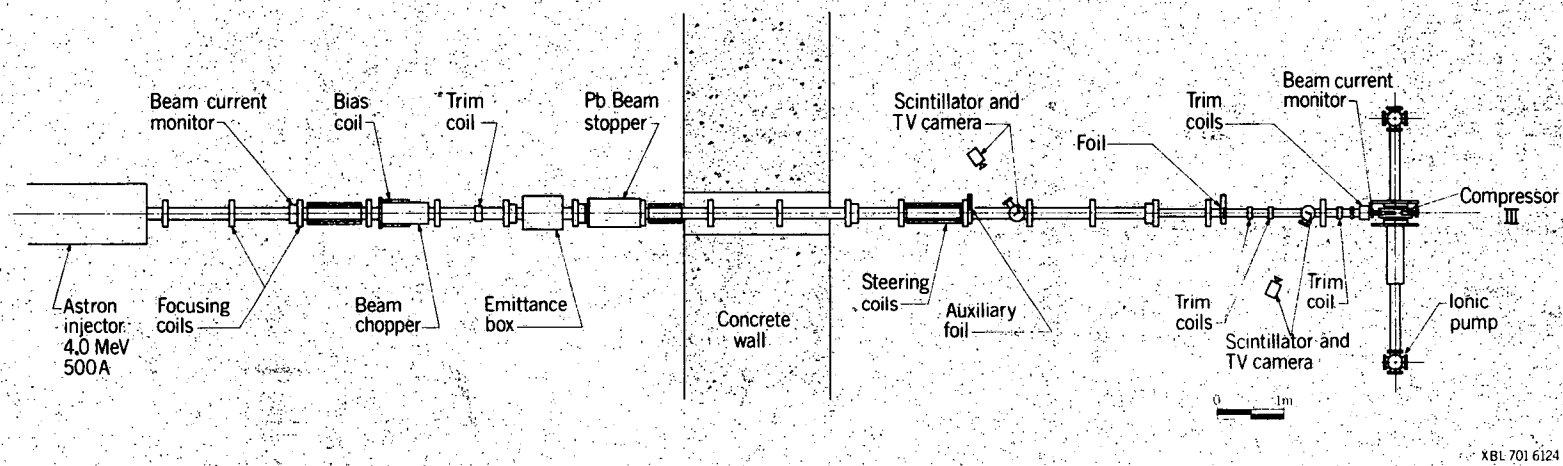
Beam current monitor
Bias coil
Trim coil
Pb Beam stopper
Scintillator and TV camera
Foil
Trim coils
Beam current monitor
Compressor III
Astron injector 4.0 MeV 500A
Focusing coils
Beam chopper
Emittance box
Concrete wall
Steering coils
Auxiliary foil
Trim coils
Scintillator and TV camera
Trim coil
Ionic pump
0
1m
XBL 701 6124

Fig. 1

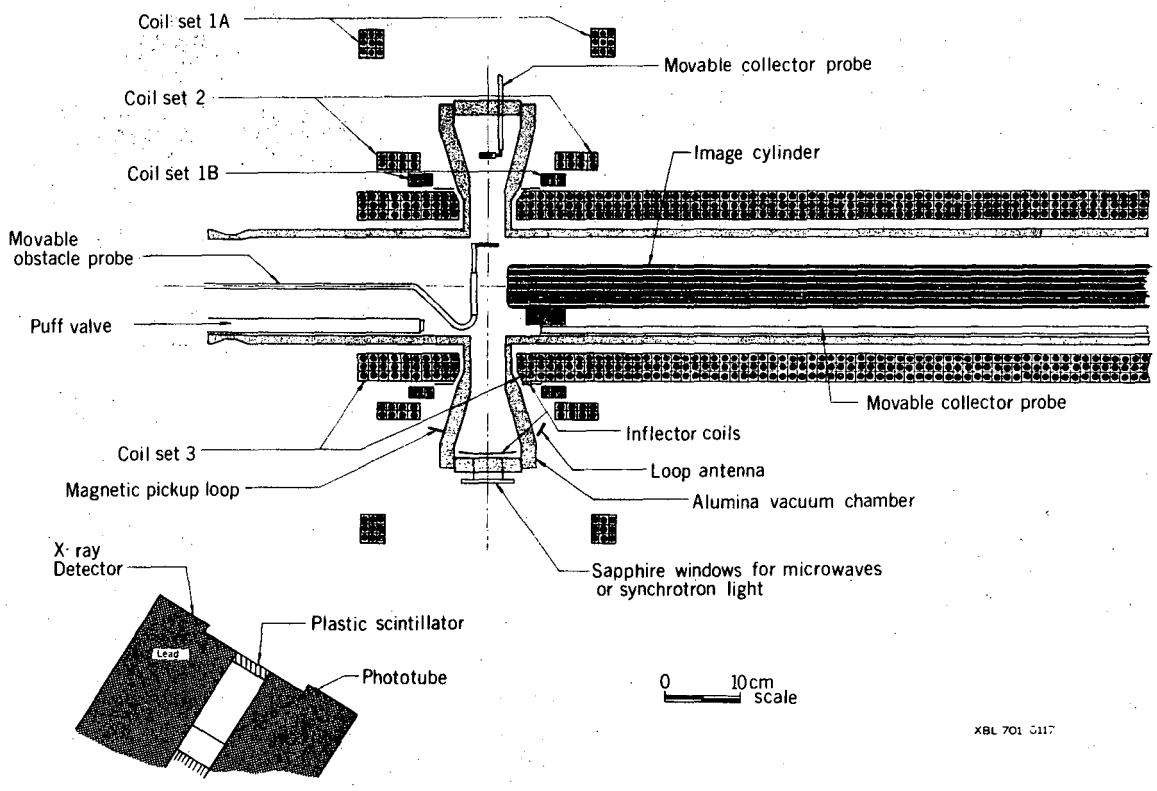
Coil set 1A
Movable collector probe
Coil set 2
Image cylinder
Coil set 1B
Movable obstacle probe
Puff valve
Movable collector probe
Inflector coils
Coil set 3
Loop antenna
Magnetic pickup loop
Alumina vacuum chamber
X-ray Detector
Sapphire windows for microwaves or synchrotron light
Plastic scintillator
Lead
Phototube
0 10cm scale
XBL 701 5117

Fig. 2

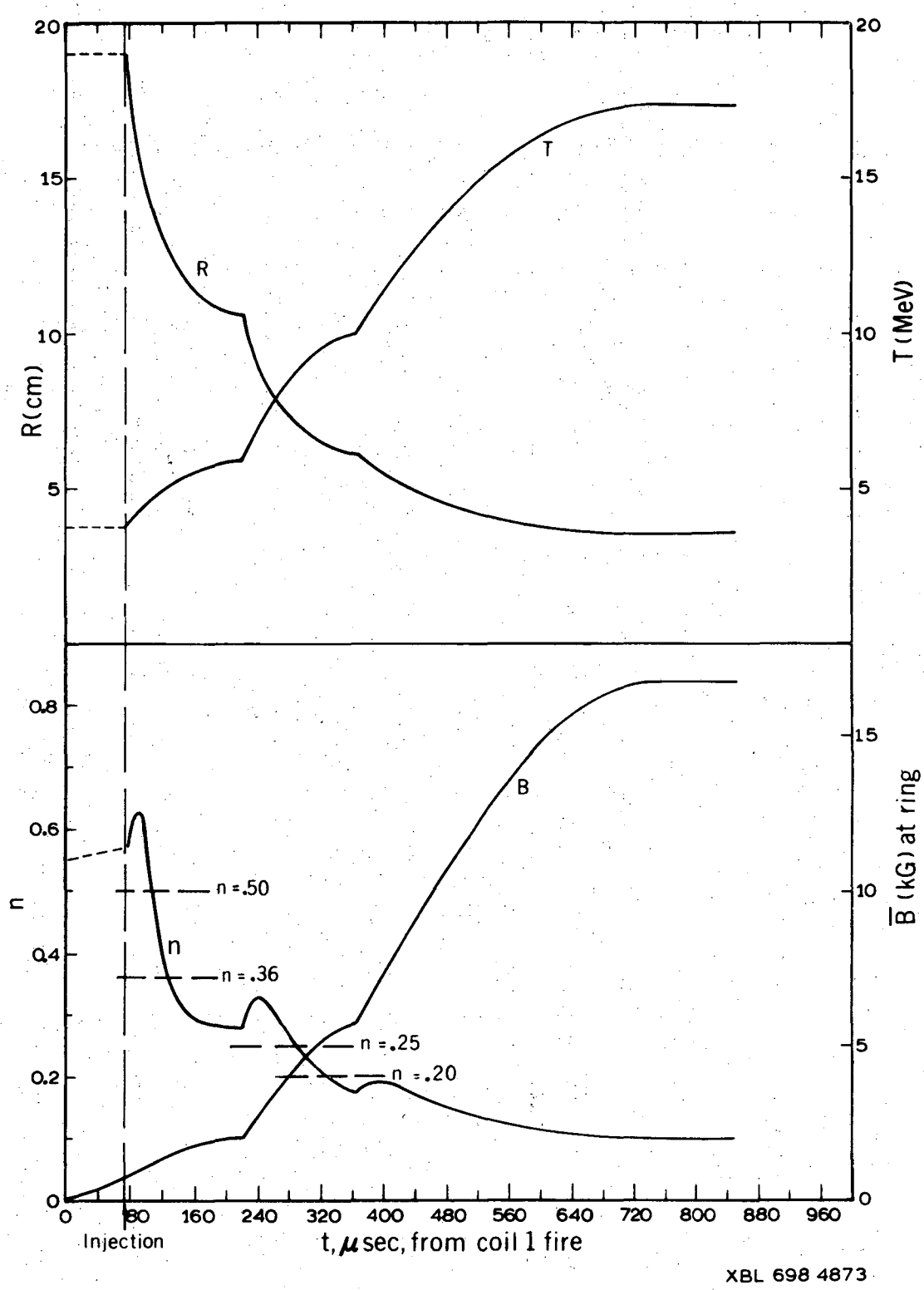
R(cm)
T (MeV)
R
T
n
B
n = .50
n = .36
n = .25
n = .20
$\bar{B}$ (kG) at ring
Injection
t, μsec, from coil 1 fire
XBL 698 4873

Fig. 3

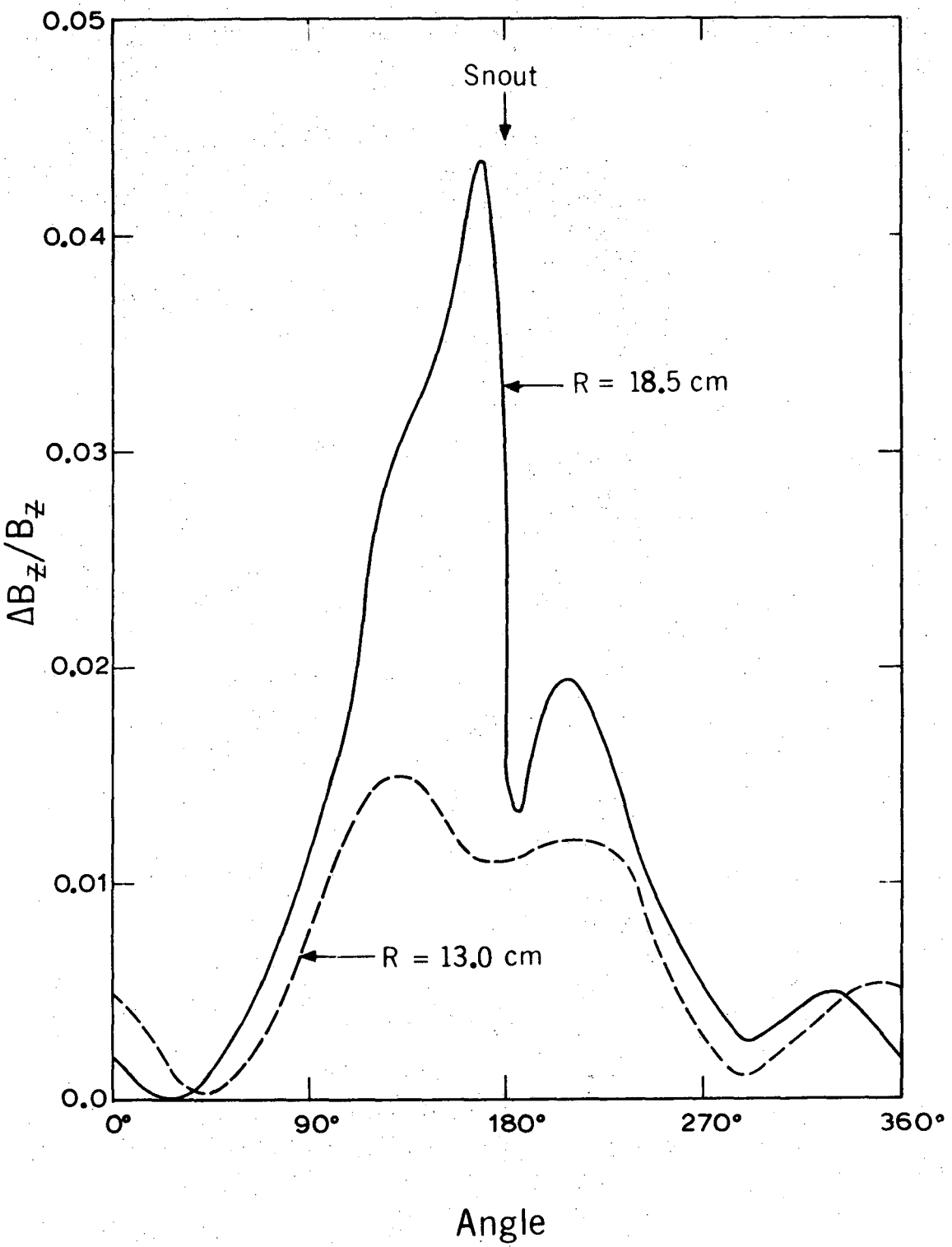

XBL 709 6240

Fig. 4

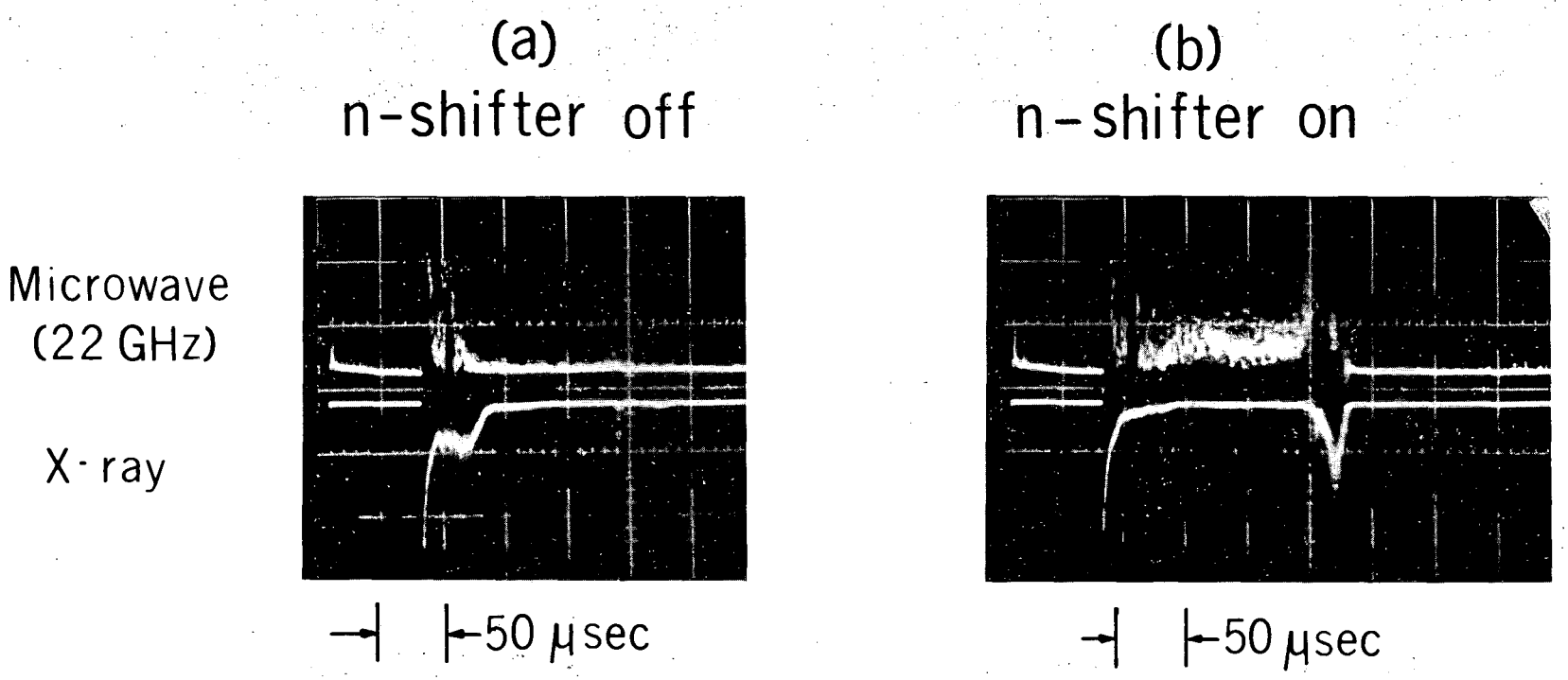

XBB 701-317

Fig. 5

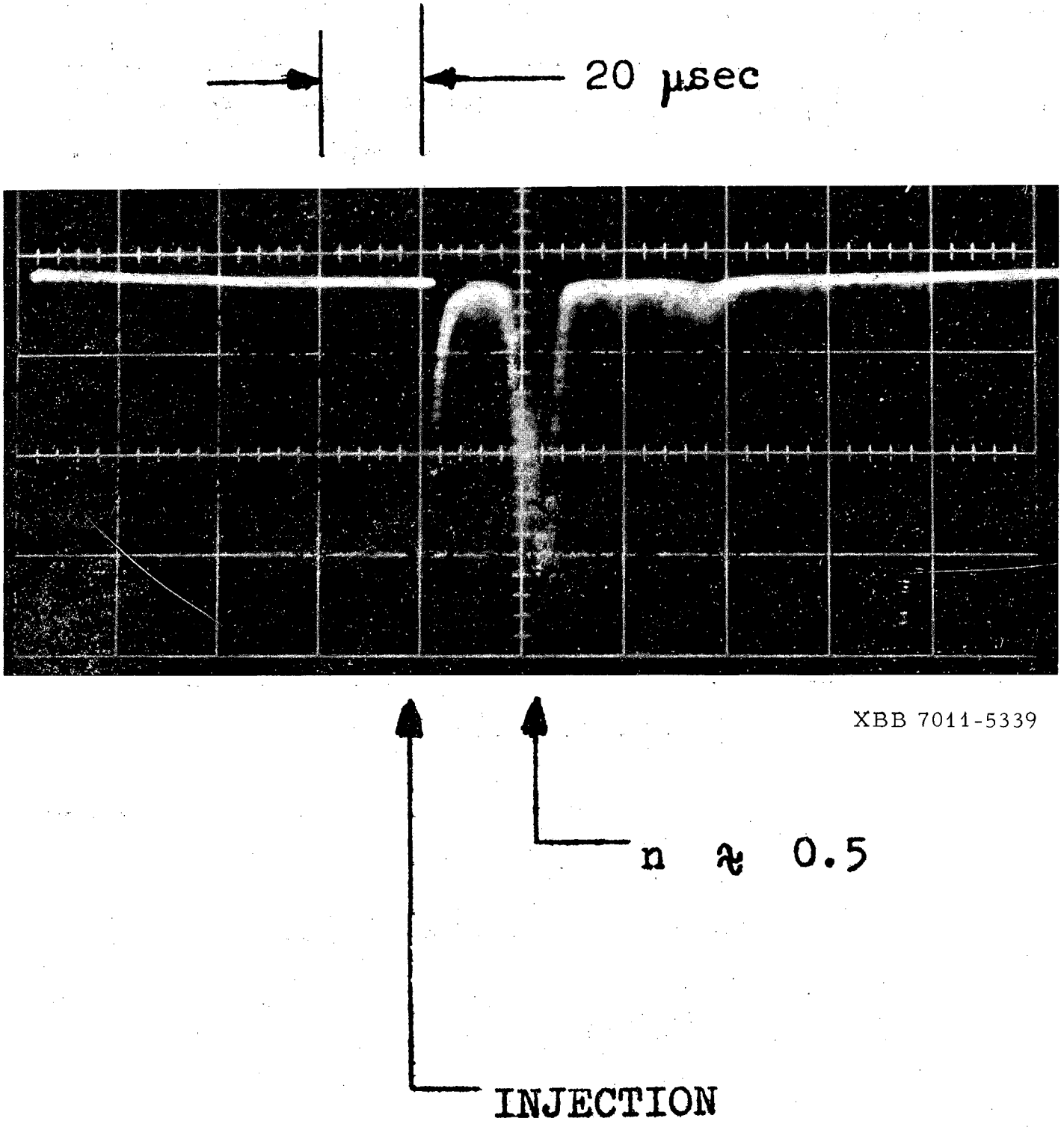

Fig. 6

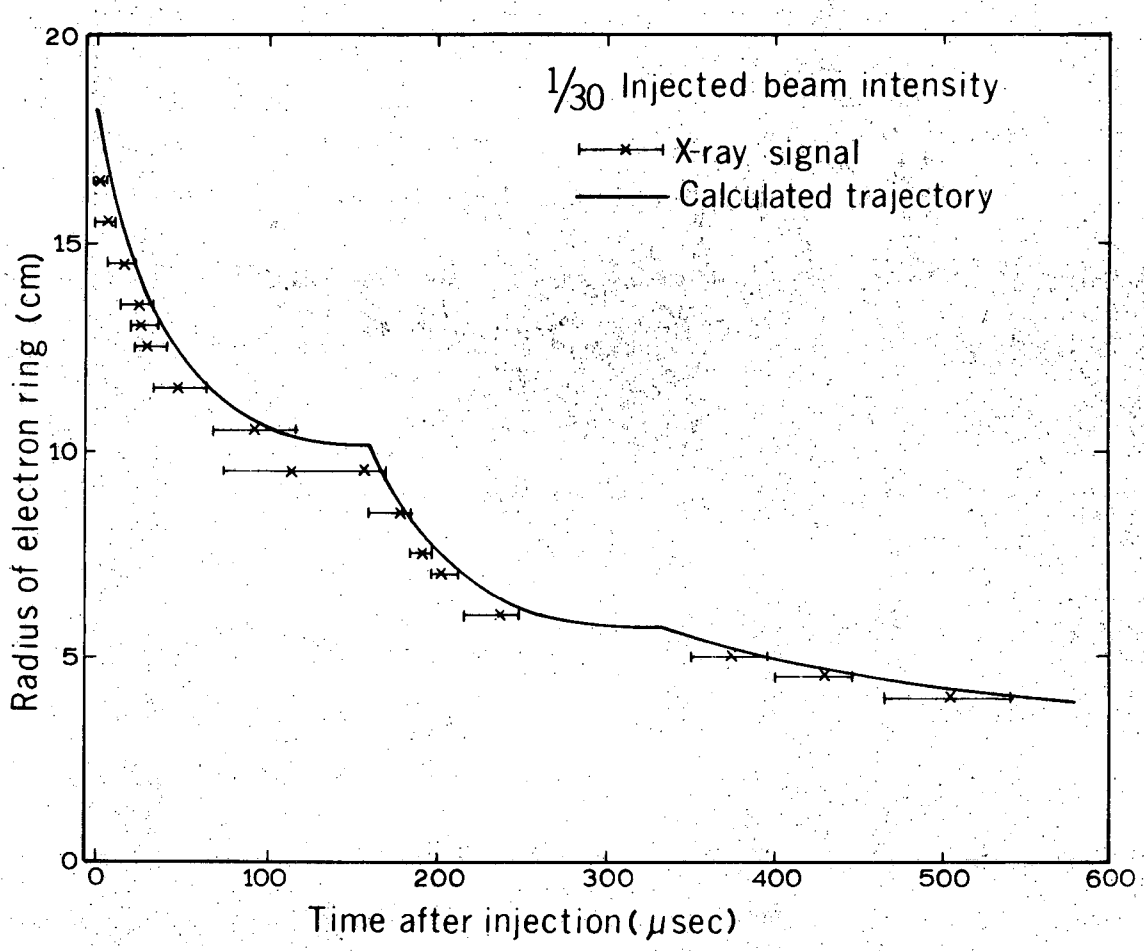

XBL 701 6133

Fig. 7

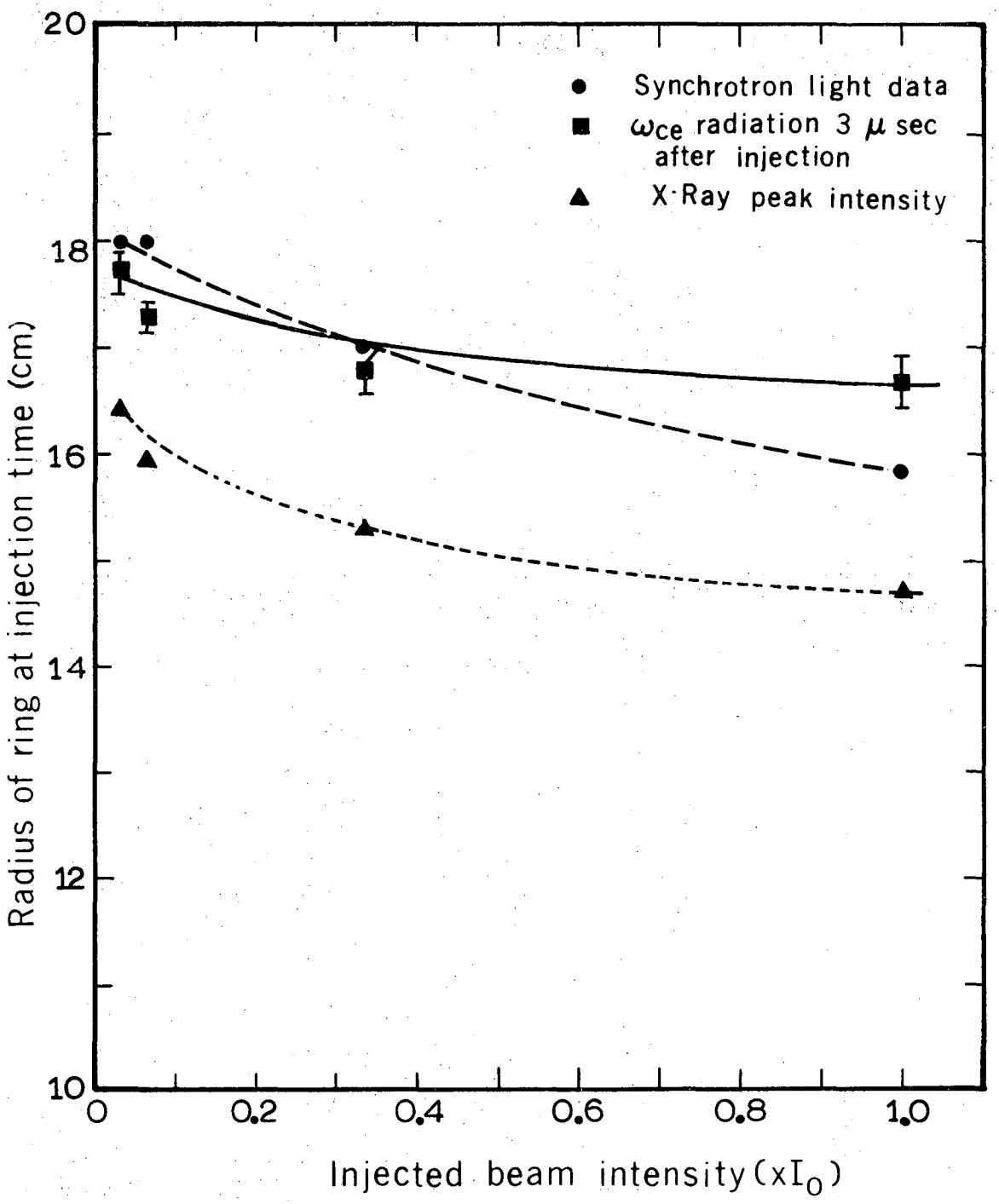

XBL 701 6114

Fig. 8

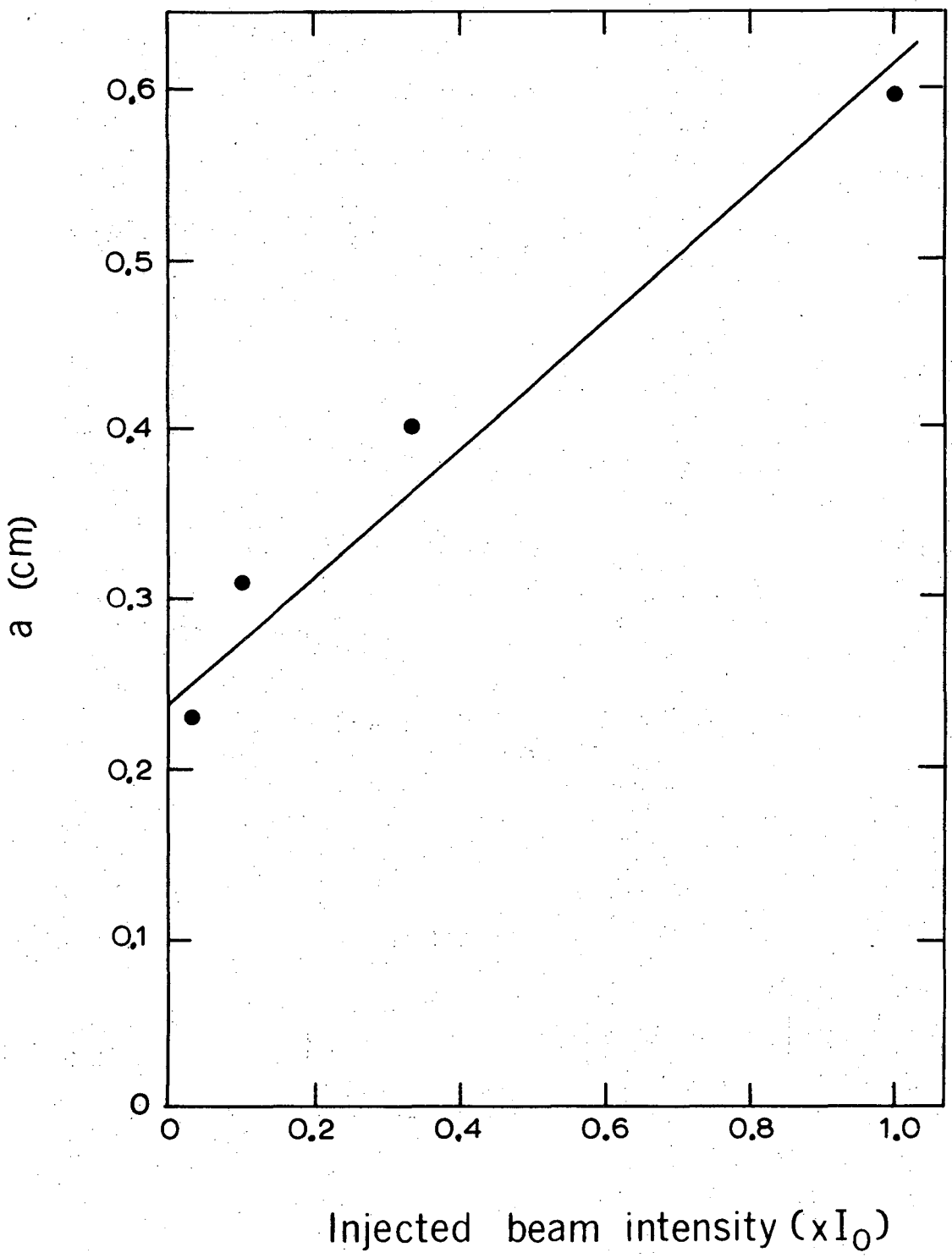

XBL 701 6131

Fig. 9

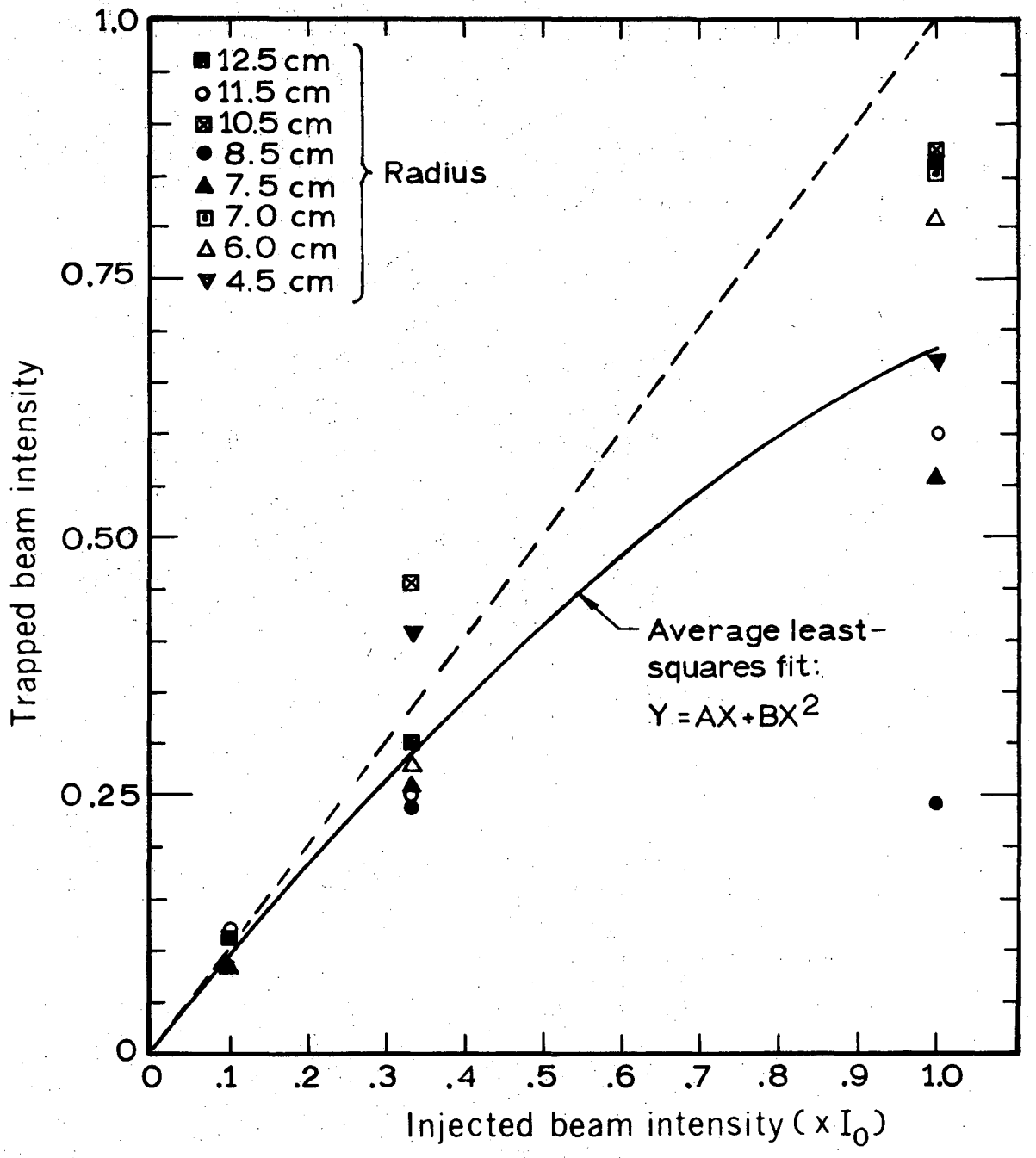

XBL 701 6113

Fig. 10

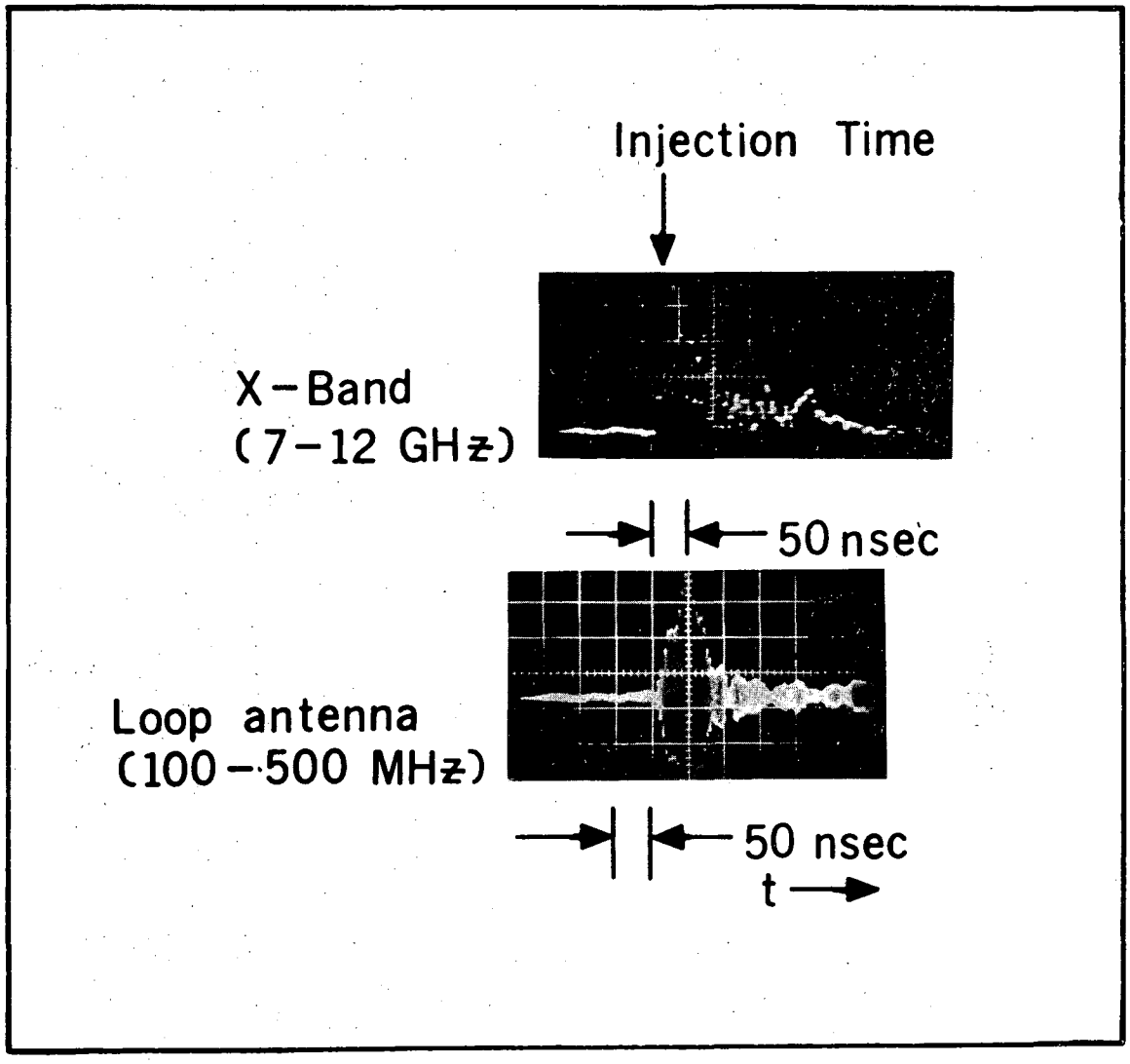

XBB 708-3742

Fig. 11

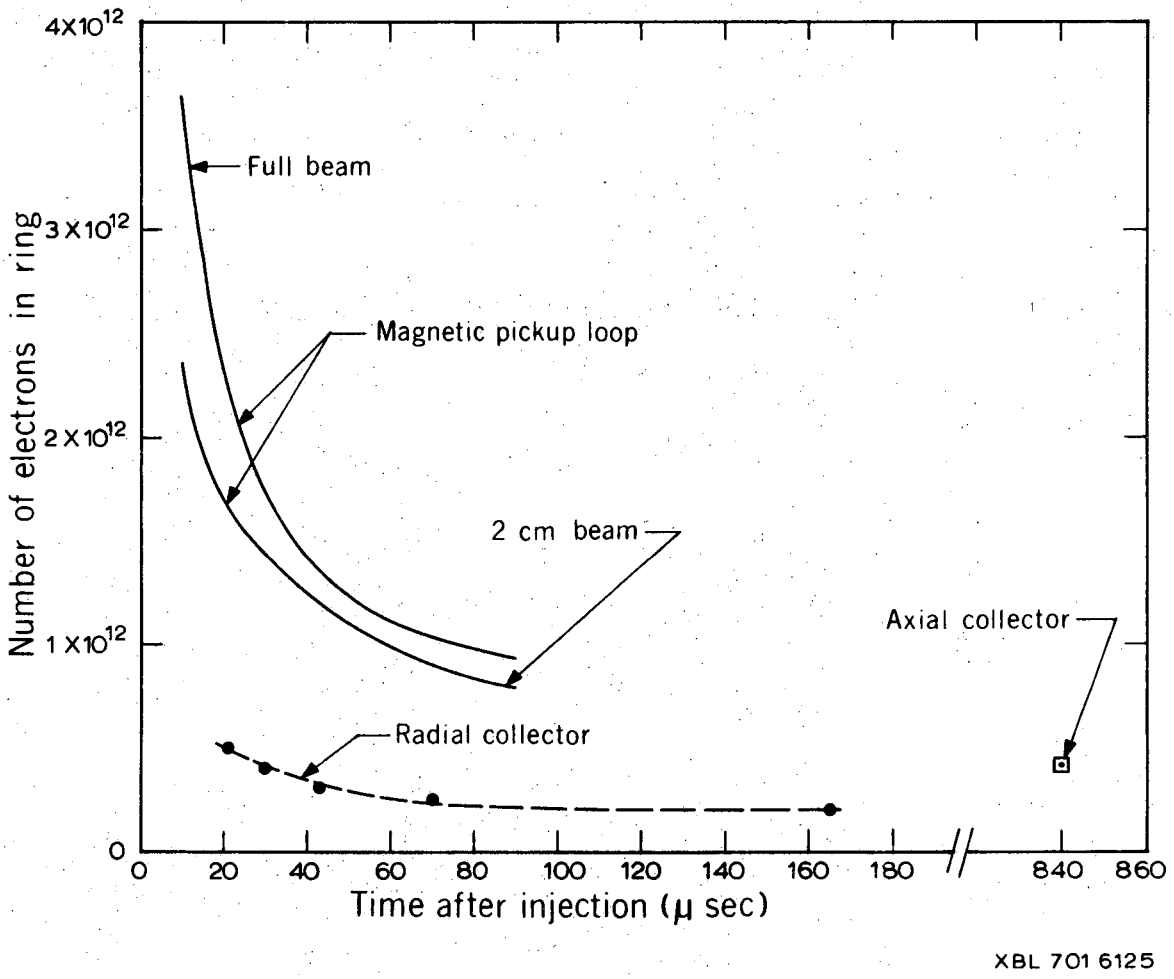
4X10^12
3X10^12
2X10^12
1X10^12
0
Number of electrons in ring
Full beam
Magnetic pickup loop
2 cm beam
Axial collector
Radial collector
0
20
40
60
80
100
120
140
160
180
840
860
Time after injection (μ sec)
XBL 701 6125

Fig. 12

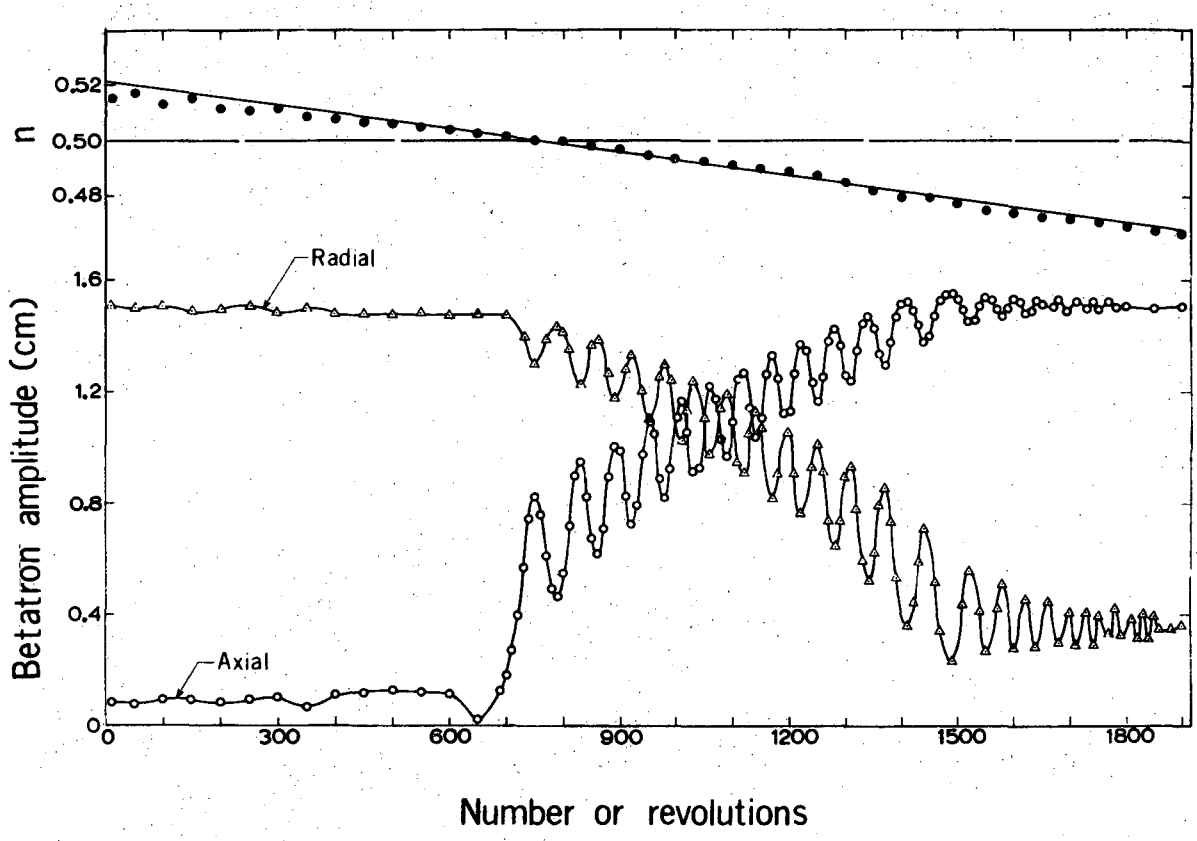
n
0.52
0.50
0.48
Radial
1.6
1.2
0.8
0.4
Axial
0
Betatron amplitude (cm)
0
300
600
900
1200
1500
1800
Number or revolutions
XBL 70106264

Fig. 13

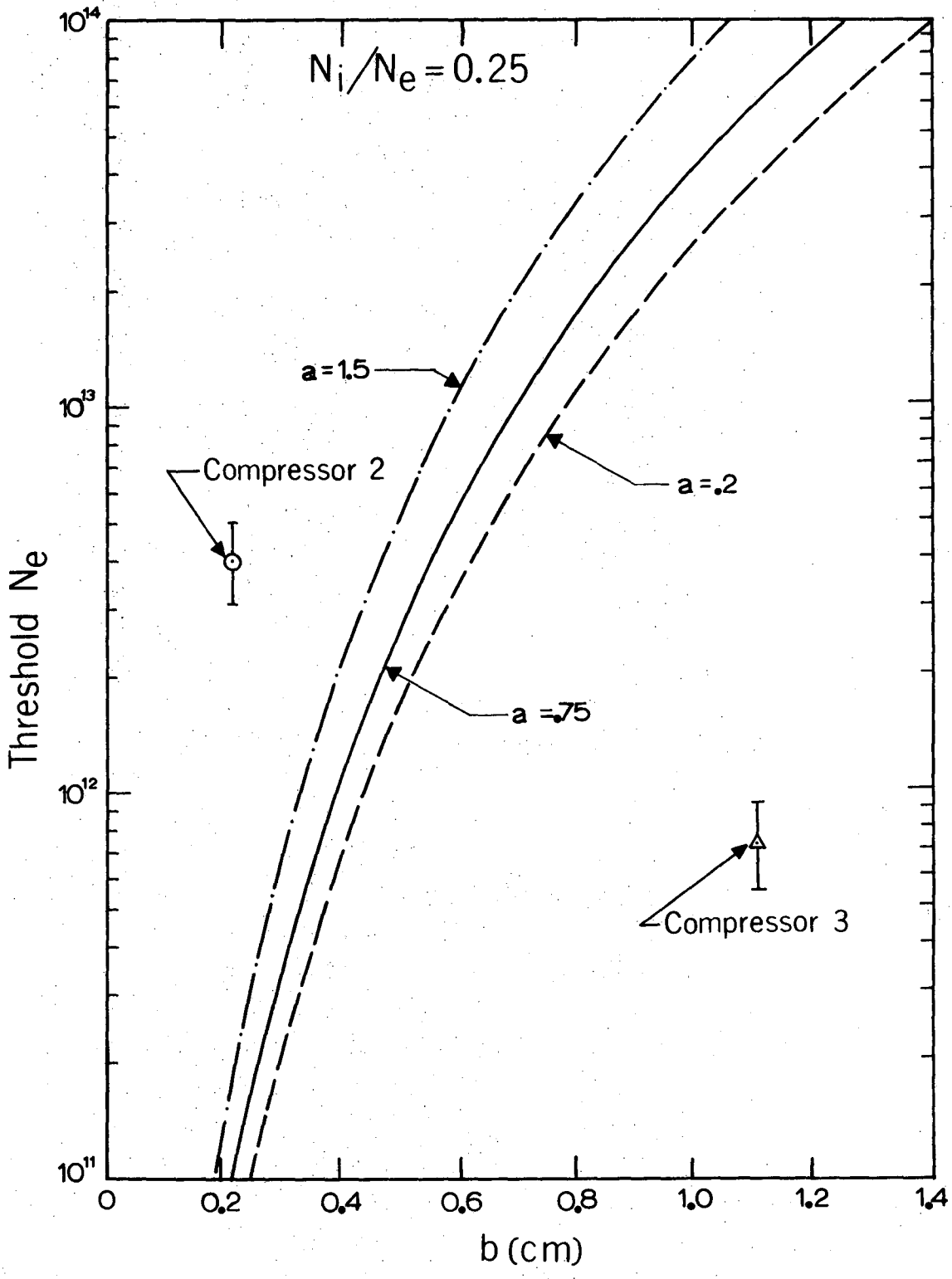

XBL 701 6126

Fig. 14

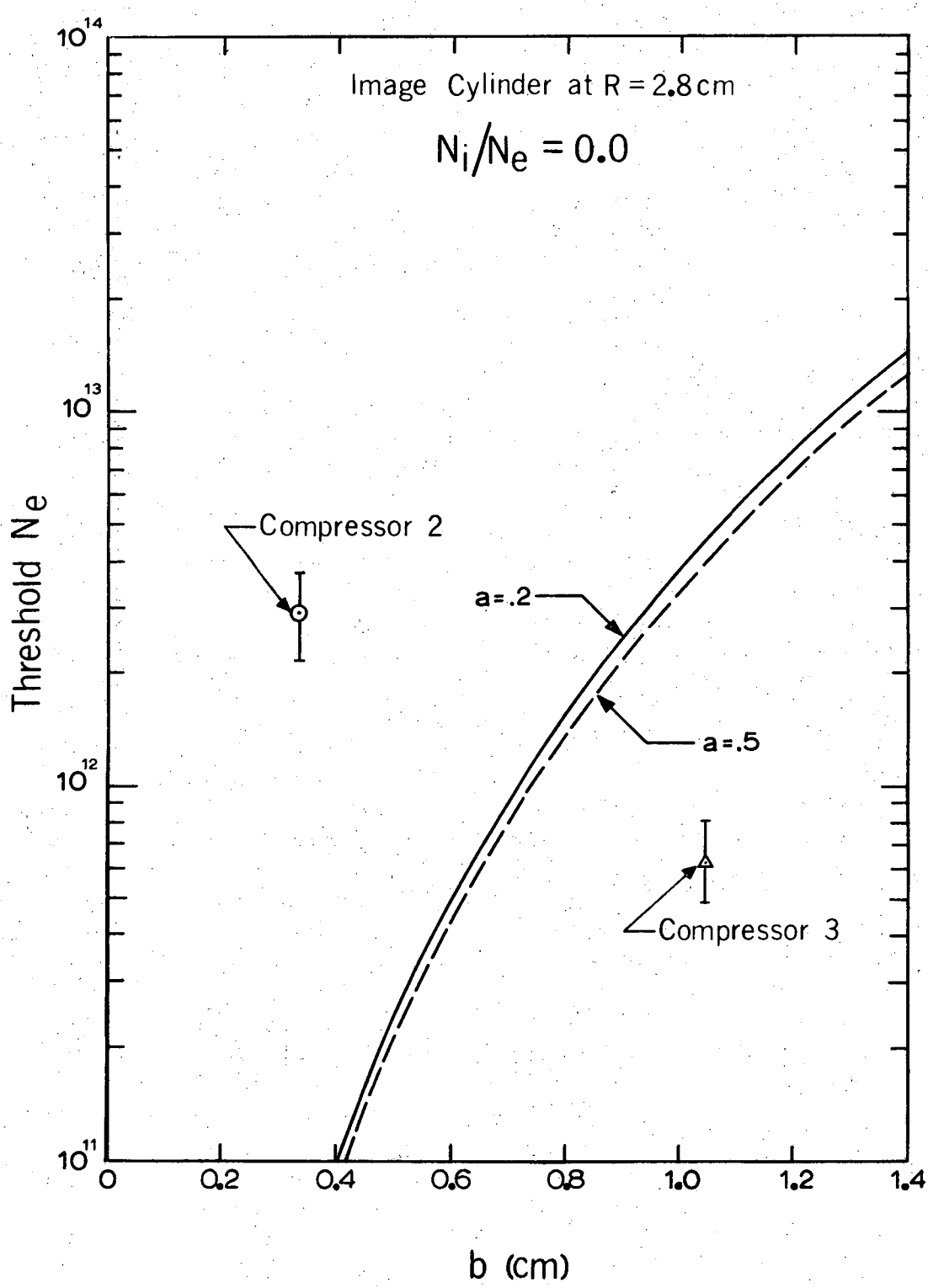

XBL 701 6132

Fig. 15

TECHNICAL INFORMATION DIVISION
LAWRENCE RADIATION LABORATORY
UNIVERSITY OF CALIFORNIA
BERKELEY, CALIFORNIA 94720